ELSEVIER

Computers in Biology and Medicine 38 (2008) 817–825

Computers in Biology and Medicine

www.intl.elsevierhealth.com/journals/cobm

Identification of ischemic heart disease via machine learning analysis on magnetocardiograms

Tanawut Tantimongcolwat[a], Thanakorn Naenna[b], Chartchalerm Isarankura-Na-Ayudhya[a], Mark J. Embrechts[c], Virapong Prachayasittikul[a,*]

[a]*Department of Clinical Microbiology, Faculty of Medical Technology, Mahidol University, 2 Prannok Road, Bangkok-noi, Bangkok 10700, Thailand*
[b]*Department of Industrial Engineering, Faculty of Engineering, Mahidol University, Nakhonpathom 73170, Thailand*
[c]*Department of Decision Sciences and Engineering Systems, Rensselaer Polytechnic Institute, Troy, NY, USA*

Received 10 May 2006; accepted 24 April 2008

Abstract

Ischemic heart disease (IHD) is predominantly the leading cause of death worldwide. Early detection of IHD may effectively prevent severity and reduce mortality rate. Recently, magnetocardiography (MCG) has been developed for the detection of heart malfunction. Although MCG is capable of monitoring the abnormal patterns of magnetic field as emitted by physiologically defective heart, data interpretation is time-consuming and requires highly trained professional. Hence, we propose an automatic method for the interpretation of IHD pattern of MCG recordings using machine learning approaches. Two types of machine learning techniques, namely back-propagation neural network (BNN) and direct kernel self-organizing map (DK-SOM), were applied to explore the IHD pattern recorded by MCG. Data sets were obtained by sequential measurement of magnetic field emitted by cardiac muscle of 125 individuals. Data were divided into training set and testing set of 74 cases and 51 cases, respectively. Predictive performance was obtained by both machine learning approaches. The BNN exhibited sensitivity of 89.7%, specificity of 54.5% and accuracy of 74.5%, while the DK-SOM provided relatively higher prediction performance with a sensitivity, specificity and accuracy of 86.2%, 72.7% and 80.4%, respectively. This finding suggests a high potential of applying machine learning approaches for high-throughput detection of IHD from MCG data.

Keywords: Ischemia; Magnetocardiography; Machine learning; Back-propagation neural network; Self-organizing map

1. Introduction

Heart diseases are the leading cause of death worldwide. Heart malfunction usually rises from ischemia due to inadequate blood supply to the cardiac muscles. Long-term deficiency of oxygen and nutrients of heart musculature leads to damage of cardiac tissue which ultimately culminates in heart attack and death. Early diagnosis of heart ischemia is critical to help reduce the mortality rate.

Electrocardiography (ECG) is traditionally used to monitor ischemic heart disease (IHD). It demonstrates the electrophysiological activity of heart via electrodes attached on the torso surface. However, in some circumstances, ECG may be normal in patients at rest during angina. Various advanced methods have been developed to improve diagnostic performance of cardiac abnormalities, such as myocardial perfusion scintigraphy and cardiac catheterization. Nonetheless, these techniques are invasive, time-consuming and require technical experts for operation. Therefore, a non-invasive and contact-free technique, namely magnetocardiography (MCG), has been developed.

MCG is a sensitive technique that monitors the magnetic field emitted by cardiac tissues. It has been considered as a promising alternative to traditional ECG since superconducting quantum interference device (SQUID) is used as contact-free probe [1–4]. This provides high reproducibility, less signal fluctuation and better spatial resolution over ECG [5–7]. MCG has been proven to be an efficient tool for many clinical applications. It is useful to monitor fetal heart activities and shows superior efficiency to determine myocardial infarction over

* Corresponding author. Tel.: +662 418 0227; fax: +662 412 4110.
E-mail address: mtvpr@mucc.mahidol.ac.th (V. Prachayasittikul).

0010-4825/$ - see front matter © 2008 Elsevier Ltd. All rights reserved.
doi:10.1016/j.compbiomed.2008.04.009

ECG [5,8–11]. Using MCG, coronary artery disease can potentially be detected in patient presenting acute chest pain [12]. Three-dimensional localization of myocardial lesion can also be visualized by magnetic mapping of MCG [13–15]. With forementioned, interpretation of MCG remains a challenge since it requires highly experienced personnel and time-consuming.

Machine learning is a promising technique that explores previously unknown regularities and trends from diverse data sets by learning from sets of data and extrapolating the newfound knowledge on testing data [16–18]. This technique has widely been adopted for biomedical applications. Lymphocytic leukemia has successfully been identified using automatic morphological analysis via machine learning [19,20]. Normal, sickle or other abnormalities of erythrocytes can be classified by the combination of image feature analysis and machine learning procedures [21]. Furthermore, successful recognition of splice junction sites of human DNA sequences has been achieved via self-organizing map (SOM), the BNN and support vector machine (SVM) learning methods [18].

Recently, the machine learning has been applied as a tool for detection of cardiac diseases. Classification of arrhythmia from ECG data set has successfully been performed by OneR, J48 and Naïve Bayes learning algorithm [22,23]. Analysis of myocardial infarction can be achieved by SOM, the BNN and robust Bayesian classifiers [24,25]. As mentioned before, MCG provides better discriminating power between healthy and disease cases. Therefore, attempts at application of machine learning have preliminarily been performed with various algorithms on MCG by our group [26].

Herein, two machine learning methods, namely back-propagation neural network (BNN) and direct kernel self-organizing map (DK-SOM), have been demonstrated as representative of supervised and unsupervised learning techniques. Supervised learning involves learning by example pattern, while the unsupervised approach learns by discovering and adapting to structured features in the input patterns [27]. Therefore, we aim to demonstrate improved usage of the DK-SOM along with application of the BNN as tools for concurrent identification of myocardial ischemia from MCG.

2. Materials and methods

2.1. Subjects and data acquisition

MCG patterns were taken from 125 individuals. Among this, 55 patterns were from patients who had been clinically evaluated having myocardial ischemia. The remaining 70 individuals were healthy and show no evidences of cardiac abnormal symptom. The data from both patient and healthy subjects were randomly selected as training set (74 cases) and testing set (51 cases).

MCG data were acquired from 36 locations above the torso by making four sequential measurements in mutually adjacent positions. At each position, the cardiac magnetic field was recorded by nine sensors for 90 s using a sampling rate of 1000 Hz, resulting in 36 individual time series. For diagnosis of ischemia, MCG signal was recorded under default filter setting at 0.05–100 Hz. The post-processing was performed by applying digital low pass filter at 20 Hz [28,29]. For automatic classification, we used data from a time window between J-point and T-peak (J–T interval) of the cardiac cycle [30]. The J–T interval was subdivided into 32 evenly spaced points resulting in a set of 1152 descriptors from 36 MCG signals for each individual case. Therefore, the descriptors from 125 cases (testing and training) were used as input for IHD prediction (Fig. 1).

2.2. Overview of machine learning approaches

The BNN, also called multilayer perceptron, is a supervised learning method, where feeding of example input patterns together with target or output patterns is needed to train the learning network. A general BNN hierarchical network is illustrated in Fig. 2. It is comprised of one input layer, one or more hidden layers, and one output layer. Each layer contains a processing unit namely neurons or nodes [31], where the data computations and transformations take place. The connections among nodes of the layers are made for further processing and transferring of the computed data. The strength of the signal flow via each connection is expressed by a numerical value known as learning weight, wherein the path of knowledge flow is discovered. The learning process starts with a projection of each training data to each neuron in the input layer. The data are then transferred to the neurons of the hidden layer under the control of initial weights of learning, which are randomly generated and seeded to the connections. Each training pattern is propagated in a forward manner (layer-by-layer) until an output pattern is computed. Afterwards, the computed output is compared to the desired or the target output and an error value is determined. As the name infers, back-propagation neural network, the errors are fed in a backward manner (layer-by-layer) to adjust the synaptic weights of the learning network. The process is repeated several times for each pattern in the training set until the total output error converges to a minimum or until a setting limit is reached during the training iterations [27].

The DK-SOM is referred to as a traditional SOM applied on kernel transformed data. Prior to processing through SOM, the input data are introduced to the kernel transformation procedures. Kernel transformation is a class of pattern recognition algorithm, which searches for similarity among the features of the descriptors. In this study, the nonlinear characteristics of MCG are captured and hidden within the kernel before being submitted to the SOM. SOM is an unsupervised machine learning method developed by Kohonen [32–34]. It is often applied for novel detection and automated clustering of unknown data patterns based on iterative competitive learning method. Units within competitive model may be organized into one or more functional layers, in which the units in a single layer are grouped into disjoint cluster. During the learning processing, each unit within a cluster inhibits all others in the same cluster to attain the winning position. The unit receiving the largest input achieves its maximum output while all others are driven to zero. Learning is accomplished only on the winner and neighboring neurons, where weight vectors are adjusted toward the input pattern vector. No learning is taken place among the losers [27].

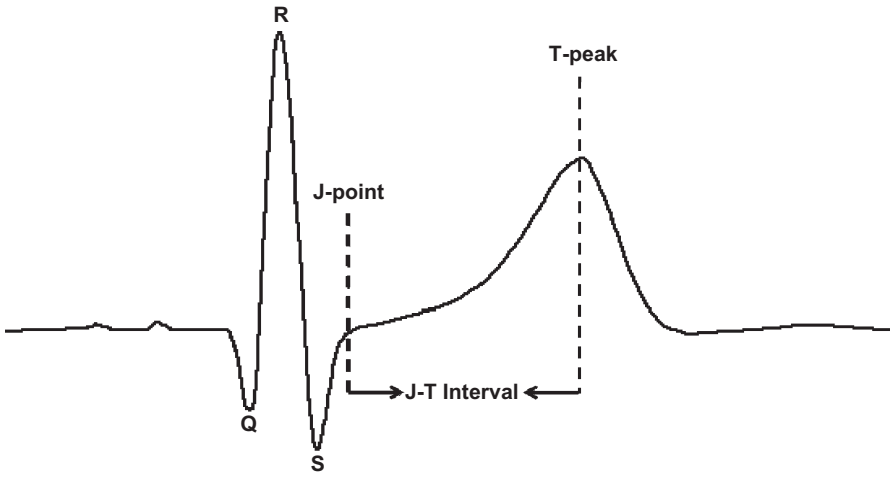

Fig. 1. MCG waveform showing *J–T* interval which was subdivided into 32 data points to serve as input for IHD prediction.

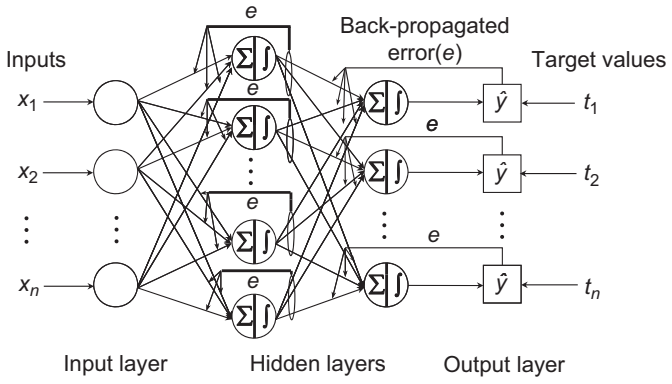

Fig. 2. Hierarchical network of BNN [19].

After training is complete, the resultant of competitive learning is presented to the output layer, which is normally arranged as either hexagonal or rectangular lattices. Usually, the hexagonal lattice is preferred because it offers a better visualization. The input data that hold the same properties are clustered together on the nearby neuron, in which the distance from one another is low. Frequently, the distances are represented by color spectrum on U-Matrix, a method for visualizing the cluster structure of the SOM. Therefore, the map is shaded to indicate the clustering tendency. Areas having low distance values in the U-Matrix form clusters, while those with high distance values on the U-Matrix indicate a cluster border [18].

2.3. BNN calculations

Supervised learning neural network calculations were performed with the back-propagation implementation of WEKA 3.4.3 [4]. The data sets were initially normalized to a range of 0 and 1 according to the following equation [35]:

$$x_{\text{norm}} = \frac{x_i - x_{\min}}{x_{\max} - x_{\min}} \tag{1}$$

where x_{norm}, x_i, $x_{\min}$ and $x_{\max}$ refer to as the normalized data, the value of each instance, the minimum value and the maximum value of the data set, respectively.

To achieve the highest prediction performance and reduction of computational time, the redundancy and multi-collinearity of descriptors were discarded with UFS version 1.8. UFS is a computer software utilizing the variable reduction algorithm namely Unsupervised Forward Selection (UFS) [36]. Briefly, the UFS starts with selection of two descriptors that exhibit the highest degree of pairwise correlation. The descriptors with squared multiple correlation coefficient ($R^2_{\max}$) less than the predefined value are selected while the rest are removed. As a result, a reduced set of 2–78 descriptors were selected from a total of 1152 descriptors. The optimal number of selected descriptors was then determined by making empirical trial-and-error learning on each data set. Sets of descriptors exhibiting the lowest predictive error were chosen as an optimal [35]. As a rule of thumb, optimal conditions for the BNN calculation were further performed by trial-and-error adjustment of various parameters including the number of nodes in hidden layer, the learning epoch, and the learning rate (η) and momentum (μ) constants. Each optimization calculation was performed for 10 runs upon adjusting initial weight of learning (random seed) from 0 to 9. The average root mean square error (RMSE) of 10 runs was subsequently used as the measure of predictive error. The optimal number of nodes in the hidden layer was determined by varying the number of hidden nodes from 1 to 30 and observing the number of node that gave the lowest RMSE. Next, the best training time was determined by varying the training time or learning epoch at the optimal number of hidden nodes. As before, the training time that gave the lowest RMSE was chosen. Finally, learning rate and momentum were simultaneously adjusted, the pair giving the lowest predictive error was chosen as optimal.

2.4. DK-SOM calculations

The DK-SOM calculations were carried out with the Analyze/StripMiner software which was developed in-house [37]. In order to improve the prediction performance, kernel transformation was performed on the data set as data transformation during the preprocessing step. This procedure was referred to

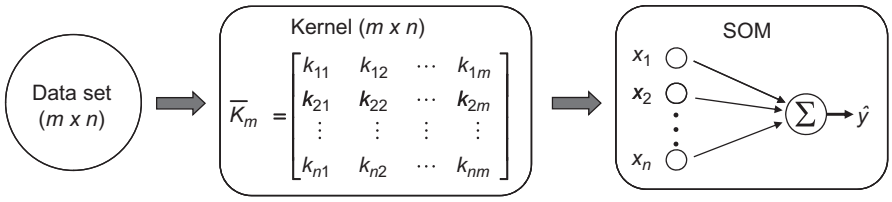

Fig. 3. Schematic illustration of DK-SOM operation.

as a direct kernel method. The nonlinear property of input data was captured and hidden in the kernel. Next, the traditional SOM calculation was applied on the kernel transformed data. The training procedure was divided into two phases, an ordering phase and a fine-tuning phase. The weights of learning were obtained by competitive learning while the winning neuron and its neighbors were updated according to the following equation:

$$\overset{\rho}{w}_{m}^{\text{new}} = (1-\alpha)\,\overset{\rho}{w}_{m}^{\text{old}} + \alpha\,\overset{\rho}{x}_{m} \tag{2}$$

where $\overset{\rho}{x}_{m}$ is a pattern vector with m feature, α is the learning parameter and $\overset{\rho}{w}$ represents the weight vector.

During the ordering phase, $\overset{\rho}{x}_{m}$ was presented at random while α was gradually reduced from 0.9 to 0.1. In addition, the neighborhood size was reduced from 6 to 1 on a hexagonal grid in a linear fashion. After 20,000 iterations, the ordering phase was terminated. In the second fine-tuning phase, α was reduced from 0.1 to 0.01 in a linear fashion with predefined learning iteration of 50,000. In the testing period, the same kernel transformation procedure was applied to the testing set generating a proper dimension of the data. The resulting weights from the training process were then challenged on the kernel transformed testing set. Finally, the prediction performance was determined on a typical 9 × 18 hexagonal grid (U-Matrix). The calculation processes are schematically summarized in Fig. 3.

3. Results

3.1. BNN parameter optimization

Optimization of the neural network architecture was carried out by determining various parameters in a trial-and-error manner using RMSE as a measure of error. This included the number of descriptors, the number of nodes in hidden layer, the number of learning epochs and the size of learning rate and momentum. For each parameter calculation, 10 runs were performed and the averages of the RMSE were calculated. Parameter exhibiting the lowest RMSE was then chosen as an optimal value.

By making a plot of RMSE versus the number of descriptors selected by UFS (Fig. 4), the optimal number of descriptors could be determined. It is observed that the number of descriptor of 12 generated minimal predictive error. Thus, it was chosen as the optimal number of descriptors. Next, the optimal number of nodes in the hidden layer was determined by plotting RMSE as a function of the number of hidden nodes. The number of hidden nodes was varied in the range of 1–30,

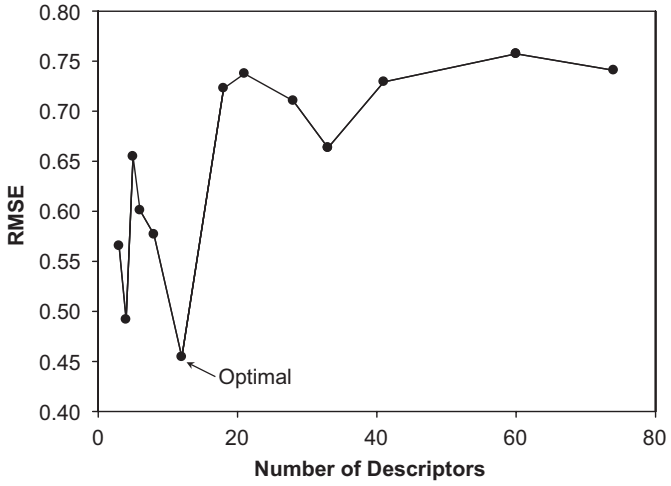

Fig. 4. Number of descriptor optimization. The number of descriptors was plotted as a function of RMSE.

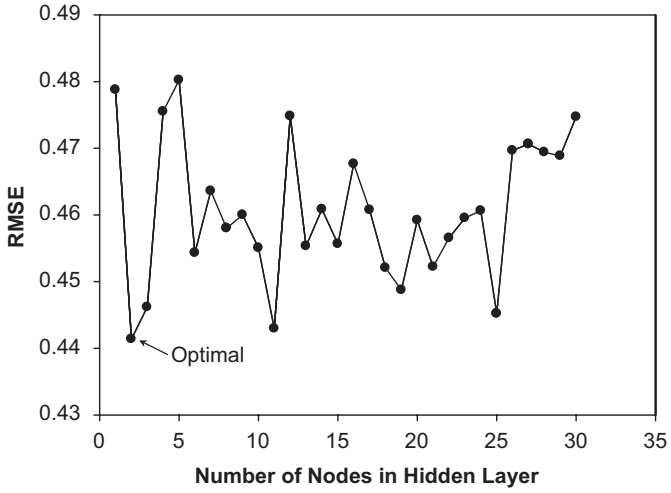

Fig. 5. Hidden node optimization. The number of nodes in hidden layer was plotted as a function of RMSE.

the corresponding average RMSEs are represented in Fig. 5. The optimal number of nodes was found to be 2 since it gave the lowest RMSE. The most efficient learning epoch was obtained by plotting RMSE versus the number of learning epoch (Fig. 6). In the same manner, the learning epoch size was varied from 50 to 1000 at interval of 50. RMSE gradually decreased upon increasing the size of the learning epoch. The lowest

RMSE was observed at 350 epochs. Beyond 350 epochs minor deviation in RMSE was observed, therefore 350 learning epoch was established as the optimum of learning epoch. The optimal learning rate and momentum were determined by making a contour plot of RMSE as a function of the learning rate and momentum (Fig. 7). The momentum and learning rate were simultaneously varied in the range of 0–1. Each line shown in the contour plot represents constant value of RMSE while the shaded boxes correspond to the RMSE values obtained from the learning procedures and fitted onto the same surface model. Good learning rate and momentum were found in the middle left region of the plot. Thus, the optimal value of learning rate and momentum were chosen to be 0.3 and 0.4, respectively. Hence, automatic analysis of myocardial ischemia was performed using the empirically determined optimal parameter settings of 2, 350, 0.3 and 0.4 for hidden node, learning epoch size, learning rate and momentum, respectively.

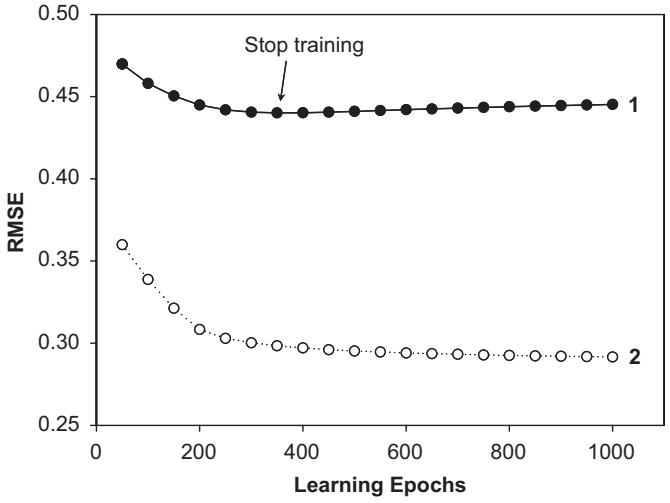

Fig. 6. Learning epoch optimization. The number of learning epoch was plotted as a functions of RMSE. Curves 1 and 2 represent the testing and training sets, respectively.

3.2. DK-SOM calculation

The direct kernel transformed data set was introduced to Kohonen's SOM with a hexagonal grid dimension of 9 × 18. The Analyze/StripMiner software package was used for this analysis. The parameter values for the DK-SOM were fine-tuned using the training set prior to testing. The results are similar to the quality of classification as achieved by the trained expert [38–40]. A typical 9 × 18 U-Matrix map based on the

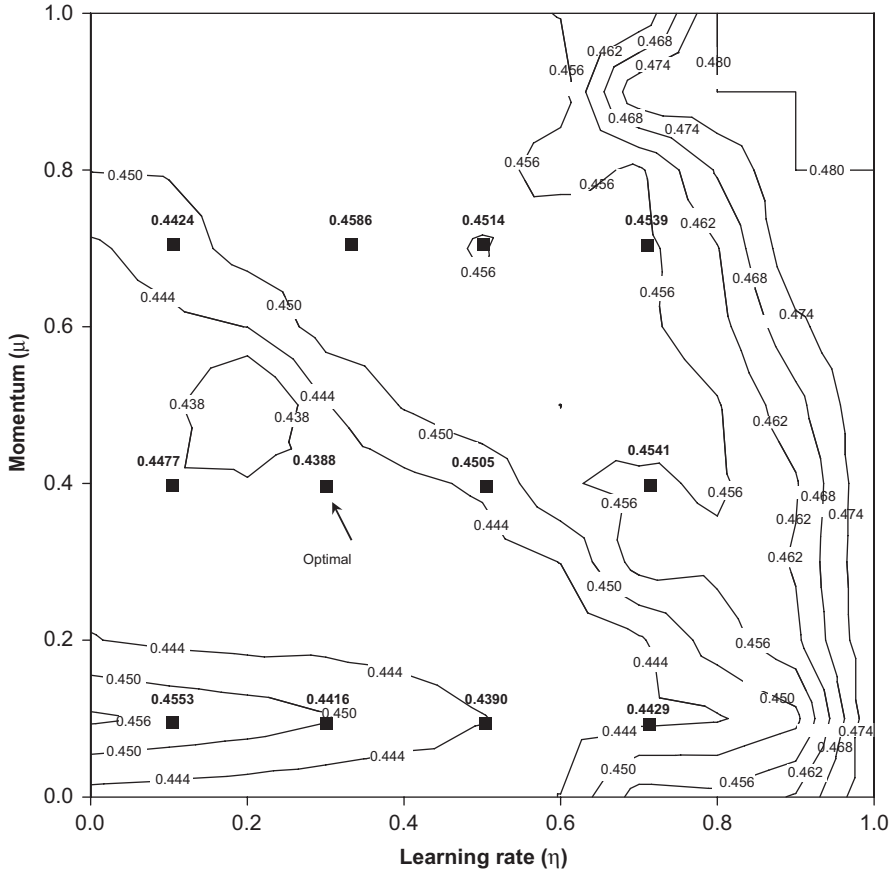

Fig. 7. Learning rate and momentum optimization. Contour plot of RMSE in testing set versus learning rate (η) and momentum (μ) for the testing set. Each line represents constant value of the RMSE, while shaded boxes represent RMSE values obtained from the training procedure and fitted onto the same surface model of the contour plot.

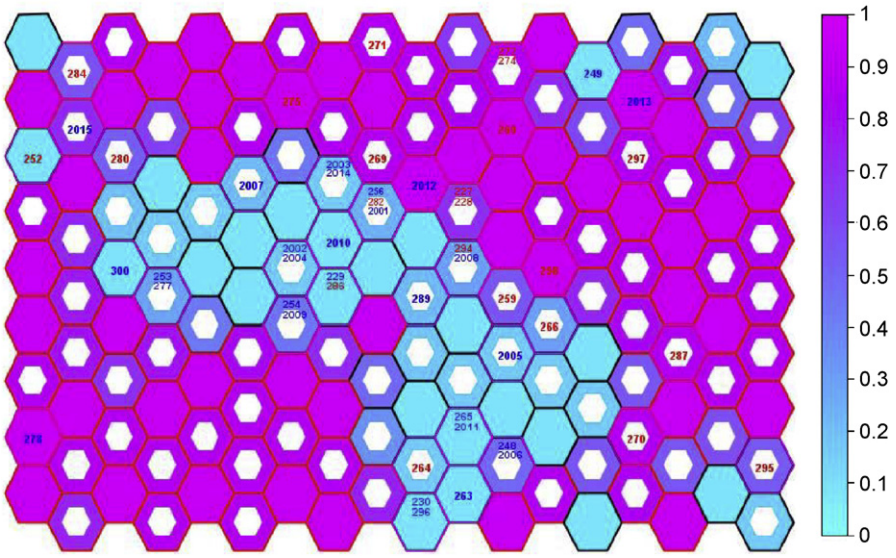

Fig. 8. Testing data together with training data are displayed on the SOM based on a 9 × 18 DK-SOM. Light colored cells indicate healthy cases, and dark colored cells show IHD cases. Patient IDs for the test cases are displayed as well.

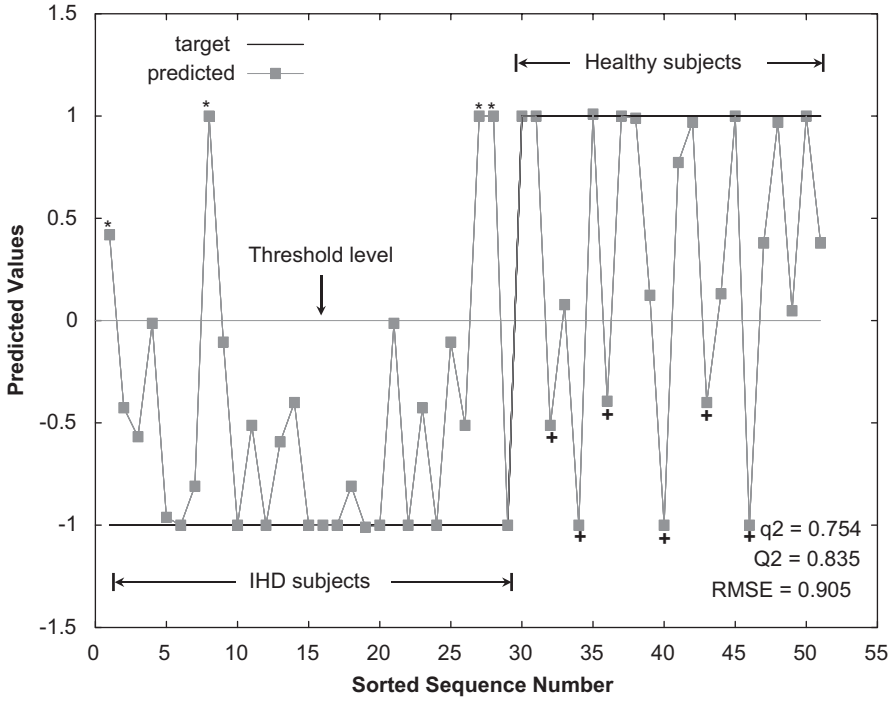

Fig. 9. Error plot represents predictive values versus actual values of 51 testing cases. Target value for IHD is −1, while 1 stands for healthy control. The predicted values labeled with star (*) and plus sign (+) indicate the misclassification of IHD and healthy subjects, respectively.

direct kernel SOM is shown in Fig. 8. Dark hexagons indicate disease cases, while light hexagons represent healthy cases. Fully colored hexagons indicate the position of training data, whereas white- and dark-shaded numbers refer to the pattern identifiers of healthy and disease test cases. As represented on the U-Matrix map, a discrete organization between the healthy and the disease cases was observed. Nevertheless, some misclassifications were found at the boundary regions of the map. The prediction results shown in the U-Matrix map are illustrated in the error plot (Fig. 9). The designed prediction performance can be achieved by changing the decision threshold. Therefore, possible outcomes were shown in ROC curve in which true positives were plotted against false negatives (Fig. 10). The closer the curve to the left and to the top border of the ROC plot, the higher the predictive performance of the models. In fact, any increase in sensitivity is accompanied by the decrease

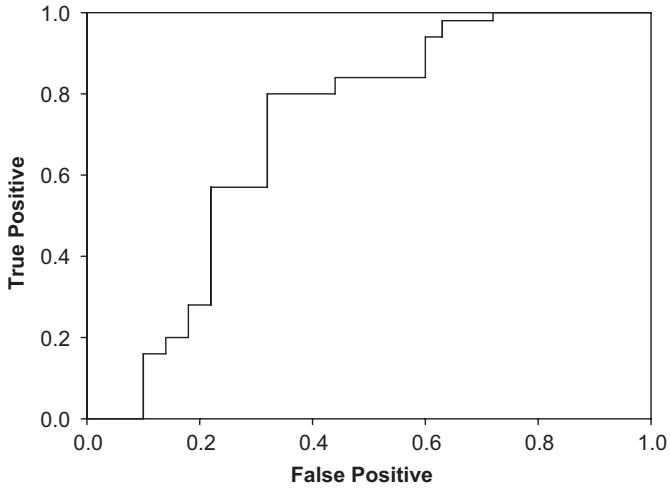

Fig. 10. ROC curve of DK-SOM model.

Table 1
Confusion matrix represents prediction results obtained from BNN and DK-SOM machine learning

Subjects	IHD	Control	Total
IHD	26 (25)	3 (4)	29
Control	10 (6)	12 (16)	22

Numbers in the bracket were made by DK-SOM while the outsides were acquired by BNN.

Table 2
The prediction performance generated by both machine learning approaches (DK-SOM and BNN)

Machine learnings	Accuracy[a] (%)	Sensitivity[b] (%)	Specificity[c] (%)
BNN	74.5	89.7	54.5
DK-SOM	80.4	86.2	72.7

[a]Accuracy = (true positive plus true negative test results)/all subjects.
[b]Sensitivity = true positive test results/all subjects with disease.
[c]Specificity = true negative tests results/all subjects without disease.

in specificity. Therefore, in this experiment, the cutoff was set as zero in order to achieve the best sensitivity and specificity (Fig. 9). The target values of disease cases and healthy controls were indicated by numerical values of −1 and 1, respectively. The predicted values falling in the region between the threshold and the target values are correctly classified, while those of misclassified are located outside the target region.

3.3. Prediction of IHD

Once the optimal conditions for machine learning were obtained, prediction of IHD was performed on the MCG testing set. As represented in the confusion matrix (Table 1), the data set of 51 testing subjects consists of 29 IHD patients and 22 healthy controls. Three IHD patients and 10 control subjects were misclassified by the BNN, while fewer misclassifications were obtained by the DK-SOM (four IHD patients and six control subjects). Thus, prediction accuracy of 80.4% was obtained by the DK-SOM, while 74.5% was observed from the BNN (Table 2). Furthermore, the specificity of prediction made by the DK-SOM was 72.7%, which was higher than that obtained from the BNN (54.5%). It is noteworthy that low specificity of the BNN was compensated by higher prediction sensitivity of up to nearly 90%. Both the DK-SOM and the BNN techniques presented sensitivity of up to 86.2% and 89.7%, respectively.

4. Discussion

MCG has increasingly been employed for non-invasive investigation of cardiac abnormalities. It can discriminate healthy and diseased cases at resting condition better than traditional ECG [41,42]. Regular interpretation of magnetic field map provides high values of sensitivity (83%) and specificity (96%) for differentiation of myocardial ischemia [43], which is twice higher in sensitivity and negative predictive values for detection of coronary artery disease as compared to ECG, troponin-I level and echocardiography approaches [12]. However, interpretation of MCG is time-consuming and requires highly skilled personnel. Attempts for automatic analysis of MCG have been performed. In our previous works, various machine learning algorithms have been applied on wavelet and time domains of MCG to differentiate between healthy and IHD. The DK-SOM and the direct kernel partial least square (DK-PLS) have been used as representative of unsupervised and supervised machine learning methods, respectively. Prediction accuracy has been found in the range of 71–83% [26]. A comparable result has been obtained by Fenici and coworkers [44] where utilization of T-wave extrema and effective magnetic dipole derived from magnetic field analysis in conjunction with the DK-PLS provided only 75% sensitivity and 85% specificity for detection of IHD. Moreover, regular T-wave analysis provides lesser sensitivity in the detection of coronary artery disease and abnormal clue on previous occurrence of myocardial infarction [43].

Herein, we report novel application of machine learning to predict IHD using *J–T* interval of MCG recording. Regular interpretation of *J–T* interval has been proven to provide high detection sensitivity to cardiac abnormality [45,46]. Our machine learning models reveal higher sensitivity (86.2%) and specificity (73%) for detection of IHD (Table 2). This is also attributable to the high performance of the DK-SOM on analysis of nonlinear and complex data, which is useful for pattern recognition purposes. Our data show that the BNN provides less specificity and accuracy, which on the contrary yields high sensitivity (90%). Therefore, BNN may be used initially to detect high risk individuals while false positive cases can subsequently be ruled out by the DK-SOM. Taken together, the intelligent capabilities of both the BNN and the DK-SOM offer good prospect in detecting IHD via magnetocardiograms in an automatic manner. We have demonstrated that the combined use of BNN and DK-SOM can maximize IHD screening on high risk population which serves as a beneficial assistance in MCG interpretation and rapid diagnosis.

Conflict of interest statement

None declared.

Acknowledgments

The authors sincerely acknowledge Mr. Karsten Sternickel and Prof. Bolek Szymanski for the preparation of the data set used in this study. We thank Dr. Chanin Nantasenamat for his guidance on the application of BNN. This project has partially been supported by a grant from the annual budget of Mahidol University (B.E. 2551–2555).

References

[1] H. Kanzaki, S. Nakatani, A. Kandori, K. Tsukada, K. Miyatake, A new screening method to diagnose coronary artery disease using multichannel magnetocardiogram and simple exercise, Basic Res. Cardiol. 98 (2003) 124–132.

[2] Y. Ono, A. Ishiyama, N. Kasai, S. Yamada, K. On, S. Watanabe, I. Yamaguchi, T. Miyashita, K. Tsukada, Bayesian classification of myocardial excitation abnormality using magnetocardiogram maps for mass screening, Neurol. Clin. Neurophysiol. 43 (2004) 1–5.

[3] K. Tsukada, H. Sasabuchi, T. Mitsui, Measuring technology for cardiac magneto-field using ultra-sensitive magnetic sensor for high speed and noninvasive cardiac examination, Hitachi Rev. 48 (1999) 116–119.

[4] I. Tavarozzi, S. Comani, C.D. Gratta, G.L. Romani, S.D. Luzio, D. Brisinda, S. Gallina, M. Zimarino, R. Fenici, R. Caterina, Magnetocardiography: current status and perspectives. Part I: physical principles and instrumentation, Ital. Heart J. 3 (2002) 75–85.

[5] S. Yamada, I. Yamaguchi, Magnetocardiograms in clinical medicine: unique information on cardiac ischemia, arrhythmias, and fetal diagnosis, Intern. Med. 4 (2005) 1–19.

[6] S.J. Williamson, L. Kaufmann, Biomagnetism: sources and their detection, J. Magn. Magn. Mater. 22 (1981) 147–160.

[7] H. Koch, SQUID magnetocardiography: status and perspectives, IEEE Trans. Appl. Superconductivity 11 (2001) 49–59.

[8] K. Tsukada, T. Miyashita, A. Kandori, T. Mitsui, Y. Terada, M. Sato, J. Shiono, H. Horigome, S. Yamada, I. Yamaguchi, An iso-integral mapping technique using magnetocardiogram and its possible use for diagnosis of ischemic heart disease, Int. J. Cardiovasc. Imag. 16 (2000) 55–66.

[9] R. Fenici, D. Brisinda, A.M. Meloni, Clinical application of magnetocardiography, Expert. Rev. Mol. Diagn. 5 (2005) 291–313.

[10] S. Yamada, K. Tsukada, T. Miyashita, I. Yamaguchi, Calculating integral values of the cardiac magnetic field is more sensitive to repolarization abnormalities than conducting electrocardiograms, Comput. Cardiol. 27 (2000) 371–373.

[11] H.K. Lim, N. Chung, K. Kim, Y.-G. Ko, H. Kwon, Y.H. Lee, J.-M. Kim, B. Joung, J.-B. Kim, K.K. Yu, J.-R. Cho, I.-S. Kim, Y.K. Park, Can magnetocardiography detect patients with non-ST-segment elevation myocardial infarction?, Ann. Med. 7 (2007) 1–11.

[12] J.W. Park, P.M. Hill, N. Chung, P.G. Hugenholtz, F. Jung, Magneto-cardiography predicts coronary artery disease in patients with acute chest pain, Ann. Noninv. Electrocardiol. 10 (2005) 312–323.

[13] R. Fenici, D. Brisinda, Bridging non-invasive and interventional electroanatomical imaging: role of magnetocardiography, J. Electrocardiol. 40 (2007) S47–S52.

[14] K. Tolstrup, B.E. Madsen, J.A. Ruiz, S.D. Greenwood, J. Camacho, R.J. Siegel, H.C. Gertzen, J.W. Park, P.A. Smars, Non-invasive resting magnetocardiographic imaging for rapid detection of ischemia in subjects presenting with chest pain, Cardiology 106 (2006) 270–276.

[15] K. Nakai, H. Izumoto, K. Kawazoe, J. Tsuboi, Y. Fukuhiro, T. Oka, K. Yoshioka, M. Shozushima, M. Itoh, A. Suwabe, M. Yoshizawa, Three-dimensional recovery time dispersion map by 64-channel magnetocardiography may demonstrate the location of a myocardial injury and heterogeneity of repolarization, Int. J. Cardiovasc. Imag. 22 (2006) 573–580.

[16] I.H. Witten, E. Frank, Data Mining: Practical Machine Learning Tools and Techniques with Java Implementations, Morgan Kaufmann, San Francisco, 2000.

[17] J. Han, M. Kamber, Data Mining: Concepts and Techniques, Morgan Kaufmann, San Francisco, 2001.

[18] C. Nantasenamat, T. Naenna, C. Isarankura-Na-Ayudhya, V. Prachayasittikul, Recognition of DNA splice junction via machine learning approaches, EXCLI J. 4 (2005) 114–129.

[19] D.M.U. Sabino, L.F. Costa, S.L.R. Martins, R.T. Calado, M.A. Zago, Automatic leukemia diagnosis, Acta Microsc. 12 (2003) 1–6.

[20] F. Scotti, Automatic morphological analysis for acute leukemia identification in peripheral blood microscope images, in: International Conference on Computational Intelligence for Measurement Systems and Applications, Giardini Naxos, Italy, July, 20–22 2005.

[21] L.L. Wheeless, R.D. Robinson, O.P. Lapets, C. Cox, A. Rubio, M. Weintraub, L. Benjamin, Classification of red blood cells as normal, sickle, or other abnormal, using a single image analysis feature, Cytometry 17 (1994) 159–166.

[22] E. Giakoumakis, N. Diamantidis, A learning system for ECG diagnosis expert system, in: Proceedings of Computers in Cardiology, London, UK, September 5–3, 1993.

[23] T. Soman, P. Bobbie, Classification of arrhythmia using machine learning techniques, Proceedings of the 4th International Conference on System Science and Engineering (ICOSSE 2005), Copacabana, Rio de Janeiro, Brazil, April 25–27, 2005.

[24] G. Bortolan, W. Pedrycz, An interactive framework for an analysis of ECG signals, Artif. Intell. Med. 24 (2002) 109–132.

[25] R. Bigi, D. Gregori, L. Cortigiani, A. Desideri, F.A. Chiarotto, G.M. Toffolo, Artificial neural networks and robust Bayesian classifiers for risk stratification following uncomplicated myocardial infarction, Int. J. Cardiol. 101 (2005) 481–487.

[26] M. Embrechts, B. Szymanski, K. Sternickel, T. Naenna, R. Bragaspathi, Use of machine learning for classification of magnetocardiograms, IEEE Proc. Syst. Man Cybern. 2 (2003) 1400–1405.

[27] D.W. Patterson, Artificial Neural Networks: Theory and Applications, Prentice-Hall, Singapore, 1996.

[28] I. Daubechies, Ten Lectures on Wavelets, Philadelphia, PA, 1992.

[29] M. Bick, K. Sternickel, G. Panaitov, A. Effern, Y. Zhang, H.J. Krause, SQUID gradiometry for magnetocardiography using different noise cancellation techniques, IEEE Trans. Appl. Superconductivity 11.1 (2001) 673–676.

[30] V. Froelicher, K. Shetler, E. Ashley, Better decisions through science: exercise testing scores, Prog. Cardiovasc. Dis. 44 (2002) 395–414.

[31] J. Zupan, J. Gasteiger, Neural Networks in Chemistry and Drug Design, Wiley, Weinheim, 1999.

[32] T. Kohonen, Self Organization and Associative Memory, 2nd ed., Springer, Berlin, 1988.

[33] T. Kohonen, The self-organizing map, Neurocomputing 21 (1998) 1–6.

[34] H. Ritter, T. Kohonen, Self-organizing semantic maps, Biol. Cybern. 61 (1989) 241–254.

[35] C. Nantasenamat, T. Naenna, C. Isarankura-Na-Ayudhya, V. Prachayasittikul, Quantitative prediction of imprinting factor of molecularly imprinted polymers by artificial neural network, J. Comput. Aid. Mol. Des. 19 (2005) 509–524.

[36] D.C. Whitley, M.G. Ford, Unsupervised Forward Selection: a method for eliminating redundant variables, J. Chem. Int. Comput. Sci. 40 (2000) 1160–1168.

[37] The Analyze/StripMiner, the description and the code are available at ⟨http://www.drugmining.com⟩, 2002.

[38] A. Golbraikh, A. Tropsha, Beware of q2, J. Mol. Graph. Model. 20 (2002) 269–276.

[39] R.H. Kewley, M.J. Embrechts, Data strip mining for the virtual design of pharmaceuticals with neural networks, IEEE Trans. Neural Network 11 (2000) 668–679.

[40] J.A. Swets, R.M. Dawes, J. Monahan, Better decisions through science, Sci. Am. (2000) 82–87.
[41] F.E. Smith, P. Langley, P.V. Leeuwen, B. Hailer, L. Trahms, U. Steinhoff, J.P. Bourke, A. Murray, Comparison of magnetocardiography and electrocardiography: a study of automatic measurement of dispersion of ventricular repolarization, Europace 8 (2006) 887–893.
[42] B. Hailer, I. Chaikovsky, S. Auth-Eisernitz, H. Schafer, P. Van Leeuwen, The value of magnetocardiography in patients with and without relevant stenosis of the coronary arteries using an unshielded system, Pacing Clin. Electrophysiol. 28 (2005) 8–16.
[43] R. Fenici, D. Brisinda, Predictive value of rest magnetocardiography in patients with stable angina, Int. Congr. Ser. 1300 (2007) 737–740.
[44] R. Fenici, D. Brisinda, A.M. Meloni, K. Sternickel, P. Fenici, Clinical validation of machine learning for automatic analysis of multichannel magnetocardiography, FIMH 3504 (2005) 143–152.
[45] C.I. Berul, T.L. Sweeten, A.M. Dubin, M.L. Shah, V.L. Vetter., Use of the rate-corrected JT interval for prediction of repolarization abnormalities in children, Am. J. Cardiol. 74 (1994) 1254–1257.
[46] K. On, S. Watanabe, S. Yamada, N. Takeyasu, Y. Nakagawa, H. Nishina, T. Morimoto, H. Aihara, T. Kimura, Y. Sato, K. Tsukada, A. Kandori, T. Miyashita, K. Ogata, D. Suzuki, I. Yamaguchi, K. Aonuma, Integral value of JT interval in magnetocardiography is sensitive to coronary stenosis and improves soon after coronary revascularization, Circ. J. 71 (2007) 1586–1592.

Tanawut Tantimongcolwat graduated from Faculty of Medical Technology, Mahidol University in 2000 with a first class honor in Radiological Technology. He received his Ph.D. in Medical Technology in 2004. Presently, he serves as a lecturer at the Department of Clinical Microbiology, Faculty of Medical Technology, Mahidol University.

Thanakorn Naenna is an Assistant Professor at the Department of Industrial Engineering, Faculty of Medical Technology, Mahidol University. He received his Ph.D. in Engineering Science from rensselaer Polytechnic Institute, Troy, NY, in 2003.

Chartchalerm Isarankura-Na-Ayudhya is an Associate Professor at the Department of Clinical Microbiology, Faculty of Engineering, Mahidol University. He graduated with the first class honor degree of Bachelor of Science from Rangsit University in 1994 and received his Ph.D. from Mahidol University in 2000.

Mark Julien Embrechts is an Associate Professor of Decision Sciences and Engineering Systems at Rensselaer Polytechnic Institute, Troy, NY. He graduated his Ph.D. and M.S. degrees in Nuclear Engineering from Virginia Polytechnic Institute in 1981 and 1978, respectively.

Virapong Prachayasittikul is an Associate Professor of Molecular Biology and Vice President of Mahidol University. He received his Ph.D. in Microbiology from University of Chicago, Chicago, IL, in 1983. He was granted an honorable degree of Doctor of Technology from Lund University (Sweden) in 2004.